Journal of Scientific Computing
https://doi.org/10.1007/s10915-018-0859-7

Numerical Simulation and Error Estimation of the Time-Dependent Allen–Cahn Equation on Surfaces with Radial Basis Functions

Vahid Mohammadi[1] · Davoud Mirzaei[2,3] · Mehdi Dehghan[1]

Received: 19 October 2017 / Revised: 5 August 2018 / Accepted: 13 October 2018

Abstract
In this paper a numerical simulation based on radial basis functions is presented for the time-dependent Allen–Cahn equation on surfaces with no boundary. In order to approximate the temporal variable, a first-order time splitting technique is applied. The error analysis is given when the true solution lies on appropriate Sobolev spaces defined on surfaces. The method only requires a set of scattered points on a given surface and an approximation to the surface normal vectors at these points. Besides, the approach is based on Cartesian coordinates and thus any coordinate singularity has been omitted. Some numerical results are given to illustrate the ability of the technique on sphere, torus and red blood cell as three well-known surfaces.

Keywords Allen–Cahn equation · Radial basis functions · Laplace–Beltrami operator · Time splitting scheme · Error estimate

1 Introduction

There are many phenomena in the applied and natural sciences which can be described as partial differential equations (PDEs) on surfaces. Such problems have received growing interest over the last years due to a variety of applications in meteorology, image processing, geometry, phycology, cell-biology, solidification, gravitation, and etc.

✉ Mehdi Dehghan
mdehghan@aut.ac.ir; mdehghan.aut@gmail.com

Vahid Mohammadi
v.mohammadi@aut.ac.ir

Davoud Mirzaei
d.mirzaei@sci.ui.ac.ir

[1] Department of Applied Mathematics, Faculty of Mathematics and Computer Sciences, Amirkabir University of Technology, No. 424, Hafez Ave., Tehran 15914, Iran

[2] Department of Mathematics, University of Isfahan, P.O. Box 81746-73441, Isfahan, Iran

[3] School of Mathematics, Institute for Research in Fundamental Sciences (IPM), Tehran 19395-5746, Iran

Published online: 26 October 2018

Finding an analytical solution for a PDE problem defined on a surface is not simple and in many situations it is impossible. Therefore, numerical techniques play an important role in this area of applied mathematics. Among all numerical methods, the role of meshless methods is prominent for problems on surfaces. The reason is clear: in these methods no background mesh and triangulation is required for approximation. This property will become more important when the information and known quantities are only available at scattered points on the surface. Thus, in the past two decades, the use of meshless methods has received much attention from researchers which are working in the field of numerical methods for solving PDEs on surfaces. The main advantage of these methods is easy implementation in high-dimension with arbitrary domain geometry. According to the choice of *testing space*, meshless methods (as well as the other methods) for PDEs can be divided into methods based on strong, weak and local weak forms. On the other side, the *trial space* should necessarily be constructed via a *scattered data approximation* method. The moving least squares (MLS) and the radial basis functions (RBF) can be addressed as two examples.

In these directions, there exists a resealable number of publications where a few of them are addressed below. For solving elliptic spherical PDEs, the kernel collocation method has been used in [29,36], the Galerkin method has been employed in [28,40] and a Petrov–Galerkin kernel approximation has been introduced in [35]. For solving reaction–diffusion equations on surfaces, a global RBF based method has been introduced in [20], the RBF-finite difference (RBF-FD) method has been implemented in [41] and the compact RBF-FD technique has been employed in [30]. Besides, the generalized moving least squares method was applied for spherical PDEs in [34]. This list is of course incomplete and thus we refer the reader to the bibliographies outlined in the above mentioned references.

In addition to the meshless methods, different methods such as finite differences, finite elements and finite volumes have been developed for solving PDEs on surfaces in recent years. Many of them can be classified into two types, *intrinsic methods* and *embedded, narrow-band methods* [20]. In the first group, coordinates intrinsic to the surface and a surface-based mesh to discretize the PDE will be used [8,13–15]. While in the second group, the PDE is first extended into a narrow band domain around the surface and then the extrinsic coordinates and an Euclidean-based mesh are used for discretization [1,7,32,33]. The intrinsic methods suffer from coordinate singularities but solve the PDE on its right dimension. The embedded, narrow-band methods, however, avoid coordinate singularities at the price of adding artificial boundary conditions and solving the PDE in a dimension at least one greater than that in which the PDE is posed. More details and comparisons can be found in [20].

According to the above discussion, Flyer and Wright [18,19] and Fuselier and Wright [20] proposed a new numerical scheme based on radial basis functions (RBFs) to solve PDE problems on surfaces which inherits the advantages of both intrinsic and embedded, narrow-band methods. The method uses RBFs and approximates the differential operators directly on the surface. This means that there is no need to extend quantities off the surface. Furthermore, it does not rely on any surface-based metric or intrinsic coordinate system.

In this paper, using the approach of [20] and an explicit time splitting scheme, we numerically solve the Allen–Cahn (AC) equation on a smooth, 2-dimensional compact manifold $\mathbb{M}$ embedded in $\mathbb{R}^3$. The error analysis of the method is also given when the true solutions lie in arbitrary Sobolev spaces. The AC equation is read as [4]

$$\frac{\partial u(\boldsymbol{x},t)}{\partial t} = -\frac{F'(u(\boldsymbol{x},t))}{E^2} + \Delta_{\mathbb{M}} u(\boldsymbol{x},t), \qquad \boldsymbol{x} \in \mathbb{M}, \quad 0 < t \leq T, \tag{1.1}$$

where $\Delta_{\mathbb{M}}$ is the well-known Laplace–Beltrami operator, $u(\boldsymbol{x}, t)$ represents the difference between the concentrations of the two mixture components, and $F(u) = 0.25(u^2 - 1)^2$. The constant parameter E denotes the gradient energy coefficient related to the interfacial energy.

The AC equation was first introduced by Allen and Cahn in 1979 for antiphase domain coarsening in a binary alloy [4]. This model has many applications in crystal growth [9,10], image in painting [17,31], image segmentation [5,23], and tumor growth [47] on flat surfaces.

Authors of [11] proposed a numerical method for motion by mean curvature of curves on a surface in three-dimensional space using the AC equation. A finite difference scheme has been developed for a conservative AC equation on non-flat surfaces in [25]. The conservative AC equation is also solved on flat surfaces in [24,26,42,43].

In this work, the Laplace–Beltrami operator in (1.1) is approximated using the attractive RBF technique of [20]. We complete the error analysis of this approximation for target functions in Sobolev spaces $H^{\sigma}(\mathbb{M})$ for all real values of σ with $3 < \sigma \leq 2s$, where s determines the smoothness of the underlying kernel. Moreover, we apply a time integration scheme which splits the nonlinear AC equation into a linear and a nonlinear subproblems. The linear problem is solved numerically while the nonlinear problem is handled analytically. For stability of the method, we prove some new results helping us to estimate the error bound for the full-discretized problem. The stability analysis is partly based on an important conjecture.

The outline of this manuscript can be expressed as follows: in Sect. 2, a first-order time splitting method and its application to AC equation are explained. In Sect. 3, the RBF collocation method on surfaces is reviewed. In Sect. 4, the details of the numerical simulation are provided. In Sect. 5, the stability and the error estimate of the proposed technique are given. Finally, in Sect. 6 some numerical results on sphere, torus and red blood cell are reported.

2 The Time Splitting Scheme

In this section, we apply the *sequential time splitting* technique [6,12,48] on Eq. (1.1). To be more precise, we first consider the following problem

$$\begin{cases} \dfrac{du(t)}{dt} = \mathcal{A}u(t) = (\mathcal{A}_1 + \mathcal{A}_2)\, u(t), \quad t \in (0, T], \\ u(0) = u_0, \end{cases} \tag{2.1}$$

where $u : (0, T] \to \mathbb{R}$ and $u_0 \in \mathbb{R}$. Here the operator $\mathcal{A} : \mathcal{U} \to \mathbb{R}$ is split into operators $\mathcal{A}_1$ and $\mathcal{A}_2$ and $\mathcal{U}$ is a solution space. Suppose further that Eq. (2.1) has a unique solution in $\mathcal{U}$. By dividing the time interval $[0, T]$ into M sub-intervals such that $T = M\Delta t$ where Δt is the time step and by defining $t_n := n\Delta t$, the sequential splitting method can be written as

$$\begin{cases} \dfrac{dv(t)}{dt} = \mathcal{A}_1 v(t), \quad t \in (t_n, t_{n+1}], \\ v(t_n) = u_{\text{spl}}(t_n), \\ \dfrac{du(t)}{dt} = \mathcal{A}_2 u(t), \quad t \in (t_n, t_{n+1}], \\ u(t_n) = v(t_{n+1}), \\ u_{\text{spl}}(t_{n+1}) := u(t_{n+1}), \end{cases} \tag{2.2}$$

for $n = 0, 1, 2, \ldots, M - 1$ and $u_{\text{spl}}(0) = u(0)$. Finally, $u_{\text{spl}}(t_{n+1})$ is the time difference solution of (2.1) at $t = t_{n+1}$. The sequential splitting scheme for Eq. (1.1) can now be expressed as

$$\begin{cases} \dfrac{dv(\cdot,t)}{dt} = \Delta_{\mathbb{M}} v(\cdot,t), \quad t \in (t_n, t_{n+1}], \\ v(\cdot,t_n) = u_{\text{spl}}(\cdot,t_n), \\ \dfrac{du(\cdot,t)}{dt} = -F'(u(\cdot,t))/E^2, \quad t \in (t_n, t_{n+1}], \\ u(\cdot,t_n) = v(\cdot,t_{n+1}), \\ u_{\text{spl}}(\cdot,t_{n+1}) := u(\cdot,t_{n+1}), \end{cases} \tag{2.3}$$

where $n = 0, 1, 2, \ldots, M-1$ and $u_{\text{spl}}(\cdot,0) = u(\cdot,0)$. The first initial value problem in (2.3) is discretized by the first-order explicit (the Euler time stepping) method, and the close-form solution of the second initial value problem is used to obtain the following two-step scheme:

$$u^{n*} = u^n + \Delta t \Delta_{\mathbb{M}} u^n, \tag{2.4}$$

$$u^{n+1} = \frac{u^{n*}}{\sqrt{\exp\left(-\frac{2\Delta t}{E^2}\right) + (u^{n*})^2 \left(1 - \exp\left(-\frac{2\Delta t}{E^2}\right)\right)}}, \quad n = 0, 1, \ldots, M-1, \tag{2.5}$$

where u^n is the approximate value of $u(\cdot,t_n)$, and u^{n*} is the intermediate solution. We will come back to this time stepping scheme after discussing a meshless technique based on RBFs for approximating the spatial variables in the next section.

3 RBFs Method on Surfaces

In this section, we briefly review a beautiful RBF method on surfaces for approximating the Laplace–Beltrami operator. For further details the interested reader is refereed to [20], where most materials of this section are adopted from this reference.

3.1 Continuous Surface Differential Operators

Let $\mathbb{M}$ be an embedded manifold in $\mathbb{R}^3$ with no boundary. The surface gradient is defined by

$$\nabla_{\mathbb{M}} := \mathbf{P}\nabla = (\mathbf{I} - \boldsymbol{n}\boldsymbol{n}^T)\nabla, \tag{3.1}$$

where $\boldsymbol{n}(\boldsymbol{x}) := (n_x, n_y, n_z)^T$ is the normal vector at point $\boldsymbol{x} = (x, y, z)$. In an extensive form, $\nabla_{\mathbb{M}}$ is written as

$$\nabla_{\mathbb{M}} = \begin{bmatrix} (1-n_x n_x)\dfrac{\partial}{\partial x} - n_x n_y \dfrac{\partial}{\partial y} - n_x n_z \dfrac{\partial}{\partial z} \\ -n_x n_y \dfrac{\partial}{\partial x} + (1-n_y n_y)\dfrac{\partial}{\partial y} - n_y n_z \dfrac{\partial}{\partial z} \\ -n_x n_z \dfrac{\partial}{\partial x} - n_y n_z \dfrac{\partial}{\partial y} + (1-n_z n_z)\dfrac{\partial}{\partial z} \end{bmatrix} =: \begin{bmatrix} \mathcal{G}^x \\ \mathcal{G}^y \\ \mathcal{G}^z \end{bmatrix}, \tag{3.2}$$

in which $\mathbf{P}$ projects vectors in $\mathbb{R}^3$ to $T_{\boldsymbol{x}}\mathbb{M}$, the tangent vector of $\mathbb{M}$ at $\boldsymbol{x}$. The Laplace–Beltrami operator $\Delta_{\mathbb{M}}$ is then defined by

$$\Delta_{\mathbb{M}} := \nabla_{\mathbb{M}} \cdot \nabla_{\mathbb{M}} = (\mathbf{P}\nabla)\cdot(\mathbf{P}\nabla) = \mathcal{G}^x\mathcal{G}^x + \mathcal{G}^y\mathcal{G}^y + \mathcal{G}^z\mathcal{G}^z. \tag{3.3}$$

Note that, all expressions above are in Cartesian coordinates. To obtain an analogue discrete version of the gradient and Laplace–Beltrami operators, we use a scattered data approximation method based on restricted radial basis functions on manifold $\mathbb{M}$.

3.2 Restricted Kernels on Manifolds

The restriction of a positive definite kernel from $\mathbb{R}^d$ to any submanifold $\mathbb{M}$ is a simple and straightforward way for obtaining a positive definite kernel on $\mathbb{M}$ because the restricted kernel inherits the property of positive definiteness from the original one, making it well-suited for scattered data interpolation problems [22]. Assume that $\Phi : \mathbb{R}^d \to \mathbb{R}$ is a positive definite basis function satisfying

$$c(1 + \|\omega\|^2)^{-\tau} \leq \widehat{\Phi}(\omega) \leq C(1 + \|\omega\|^2)^{-\tau}, \quad \omega \in \mathbb{R}^d, \tag{3.4}$$

for $\tau > d/2$. Here $\widehat{\Phi}$ represents the Fourier transform of Φ in $\mathbb{R}^d$. Condition (3.4) means that $\widehat{\Phi}$ decays algebraically in ω, and $\tau > d/2$ ensures the integrability of $\widehat{\Phi}$. A basis function Φ of this kind is necessarily finitely smooth and its *native space* in $\mathbb{R}^d$ is $\mathcal{N}_\Phi = H^\tau(\mathbb{R}^d)$. Details can be found in [44, Chapter 10]. The restriction of Φ on a k-dimensional submanifold $\mathbb{M}$ has $H^{\tau-(d-k)/2}(\mathbb{M})$ as its native space. (See Sect. 5 for definition of Sobolev spaces on compact manifolds.) The proof of this important result is given in [22]. See also [37,39] for the special case $\mathbb{M} = \mathbb{S}^{d-1}$. Further, we assume that Φ is radial that means that there exists a continuous function $\phi : \mathbb{R}_{\geq 0} \to \mathbb{R}$ such that $\Phi(\boldsymbol{x}) = \phi(\|\boldsymbol{x}\|_2)$ for all $\boldsymbol{x} \in \mathbb{R}^d$. Two kinds of such basis functions are listed below with their main properties:

- The Matérn (or Sobolev) function on $\mathbb{R}^d$ is defined by

$$\phi_\nu(r) = C_\nu r^{\nu-d/2} K_{\nu-d/2}(r), \quad \nu > d/2, \tag{3.5}$$

  where $C_\nu = \frac{2^{1-(\nu-d/2)}}{\Gamma(\nu-d/2)}$ and K_ν is the modified Bessel function of the second kind of order ν. The smoothness of ϕ_ν is controlled by ν. The Fourier transform of Matérn kernel $\Phi_\nu = \phi_\nu(\|\cdot\|_2)$ is

$$\widehat{\Phi}_\nu(\omega) = (1 + \|\omega\|^2)^{-\nu},$$

  which means that $\mathcal{N}_{\Phi_\nu}(\mathbb{M}) = H^{\nu-(d-k)/2}(\mathbb{M})$.
- The compactly supported positive definite Wendland's functions $\phi_{d,\ell} \in C^{2\ell}(\mathbb{R}^d)$ have Fourier transforms satisfying (3.4) with $\tau = \ell + d/2 + 1/2$ [44, Chapter 10]. Their restrictions to any k-dimensional submanifold $\mathbb{M}$ have $\mathcal{N}_{\phi_{d,\ell}}(\mathbb{M}) = H^{\ell+k/2+1/2}(\mathbb{M})$ as native space.

3.3 Discrete Surface Differential Operators

In this section, the discrete analogues of continuous operators $\nabla_\mathbb{M}$ and $\Delta_\mathbb{M}$ are obtained using the kernel interpolation problem on $\mathbb{M}$. As pointed before, the idea comes from [20]. Assume that

$$X = \{\boldsymbol{x}_1, \boldsymbol{x}_2, \ldots, \boldsymbol{x}_N\}$$

is a set of N scattered points on $\mathbb{M}$, and $u : \mathbb{M} \subset \mathbb{R}^3 \to \mathbb{R}$ is a continuous function. The RBF interpolant of u on $\mathbb{M}$ is denoted by $I_\phi u := I_{X,\phi} u$ and can be written as

$$I_\phi u(\boldsymbol{x}) := \sum_{j=1}^{N} c_j \phi(r_j(\boldsymbol{x})), \quad \boldsymbol{x} \in \mathbb{M}, \tag{3.6}$$

where $r_j(\boldsymbol{x}) = \|\boldsymbol{x} - \boldsymbol{x}_j\|_2$. According to (3.6), we have

$$\nabla_{\mathbb{M}} I_\phi u(\boldsymbol{x}) = \sum_{j=1}^{N} c_j \nabla_{\mathbb{M}} \phi(r_j(\boldsymbol{x})), \quad \boldsymbol{x} \in \mathbb{M}, \tag{3.7}$$

where $\nabla_{\mathbb{M}}\phi = [\mathcal{G}^x\phi,\ \mathcal{G}^y\phi,\ \mathcal{G}^z\phi]^T$ is calculated via (3.2) thereat

$$\frac{\partial \phi(r_j(\boldsymbol{x}))}{\partial x} = \left(x - x_j\right) \frac{\phi'(r_j(\boldsymbol{x}))}{r_j(\boldsymbol{x})}, \quad \text{and so on,}$$

where $'$ denotes differentiation with respect to r. Next, we define the following N-by-N matrices

$$\begin{aligned} B_X^x &= \left[\mathcal{G}^x \phi(r_j(\boldsymbol{x}))\big|_{\boldsymbol{x}=\boldsymbol{x}_k}\right], \quad k, j = 1, \ldots, N, \\ B_X^y &= \left[\mathcal{G}^y \phi(r_j(\boldsymbol{x}))\big|_{\boldsymbol{x}=\boldsymbol{x}_k}\right], \quad k, j = 1, \ldots, N, \\ B_X^z &= \left[\mathcal{G}^z \phi(r_j(\boldsymbol{x}))\big|_{\boldsymbol{x}=\boldsymbol{x}_k}\right], \quad k, j = 1, \ldots, N, \end{aligned}$$

to obtain

$$\begin{aligned} \left(\mathcal{G}^x I_\phi u\right)|_X &= B_X^x \boldsymbol{c} = \left(B_X^x A_X^{-1}\right) u_X =: G_X^x u_X, \\ \left(\mathcal{G}^y I_\phi u\right)|_X &= B_X^y \boldsymbol{c} = \left(B_X^y A_X^{-1}\right) u_X =: G_X^y u_X, \\ \left(\mathcal{G}^z I_\phi u\right)|_X &= B_X^z \boldsymbol{c} = \left(B_X^z A_X^{-1}\right) u_X =: G_X^z u_X, \end{aligned} \tag{3.8}$$

where $A_X = \left[\phi(r_j(\boldsymbol{x}_k))\right]$, $j, k = 1, \ldots, N$, $\boldsymbol{c} = [c_1, \ldots, c_N]^T$ and u_X is a column vector containing values $u(\boldsymbol{x}_j)$ for $j = 1, \ldots, N$. Now, a discrete Laplace–Beltrami matrix is define by

$$L_X := G_X^x G_X^x + G_X^y G_X^y + G_X^z G_X^z,$$

which approximates the operator $\Delta_{\mathbb{M}}$ on data set X. Theoretical results will be reviewed in Sect. 5 to show how well L_X approximates $\Delta_{\mathbb{M}}$.

4 The Full-Discrete Problem

In Sect. 2, Eq. (1.1) was converted to two-step semi-discrete Eqs. (2.4)–(2.5). The full-discrete system of equations can be obtained as

$$U_X^{n*} = U_X^n + \Delta t L_X U_X^n, \tag{4.1}$$

$$U_X^{n+1} = \frac{U_X^{n*}}{\sqrt{\exp\left(-\frac{2\Delta t}{E^2}\right) + (U_X^{n*})^2 \left(1 - \exp\left(-\frac{2\Delta t}{E^2}\right)\right)}}, \quad n = 0, 1, \ldots, M-1, \tag{4.2}$$

where the continuous operator $\Delta_{\mathbb{M}}$ is replaced by matrix L_X and the continuous functions u^n are replaced by N-vectors U_X^n. Note that, in (4.2) all mathematical operators are interpreted componentwise. Equation (4.1) is the usual forward Euler scheme and thus should be *conditionally stable*, instead no matrix inversion or assumption on solvability is required. The stability condition as well as the full order of convergence of the method will be derived in the next section.

5 Error Estimate

This section provides an error estimate for the proposed method. First, we need some definitions and preliminaries. The following definition expresses Sobolev spaces on a compact manifold $\mathbb{M}$ [20]. For the special case $\mathbb{M} = \mathbb{S}^{d-1}$ see [27].

Definition 5.1 Suppose that $\mathbb{M} \subset \mathbb{R}^d$ be a compact manifold of dimension k. Let $\tilde{A} = \{(\tilde{\Psi}_j, \tilde{U}_j)\}$, $j = 1, 2, \ldots, J$ be an atlas of slice charts for $\mathbb{M}$, and let $A = \{(\Psi_j, U_j)\}$ be the associated intrinsic atlas. Now let $\{\chi_j\}$ be a partition of unity subordinate to $\{\tilde{U}_j\}$. If u is a function defined on $\mathbb{M}$, the projection $\pi_j(u) : \mathbb{R}^k \longrightarrow \mathbb{R}$ is defined by

$$\pi_j(u) = \begin{cases} \chi_j u(\Psi_j^{-1}(y)), & y \in B'(0,1), \\ 0, & \text{otherwise} \end{cases}$$

in which $B'(0,1) = \{\boldsymbol{y} = (y_1, \ldots, y_d)^T \in B(0,1) : y_{k+1} = \cdots = y_d = 0\}$ can be viewed as a copy of an open ball in $\mathbb{R}^k$. With this construction, Sobolev spaces for $1 \leq p < \infty$ and $s \geq 0$ can be defined via the following norms

$$\|u\|_{W_p^s(\mathbb{M})} := \left(\sum_{j=1}^{J} \|\pi_j(u)\|^2_{W_p^s(\mathbb{R}^k)} \right)^{\frac{1}{2}},$$

and the Sobolev spaces $W_p^s(\mathbb{M})$ can be defined as follows

$$W_p^s(\mathbb{M}) = \left\{ u \in L_p(\mathbb{M}) : \pi_j(u) \in W_p^s(\mathbb{R}^k), \quad j = 1, 2, \ldots, J \right\},$$

where $W_p^s(\mathbb{R}^k)$ is the Sobolev spaces of order s with respect to p-norm on $\mathbb{R}^k$. The case $p = \infty$ can be defined in similar manner. In case $p = 2$, the space is Hilbert and the notation $H^s(\mathbb{M})$ is usually used instead of $W_2^s(\mathbb{M})$ and its norm is induced by the inner product

$$\langle u, v \rangle_{H^s(\mathbb{M})} := \sum_{j=1}^{J} \langle \pi_j(u), \pi_j(v) \rangle_{H^s(\mathbb{R}^k)}.$$

The order of convergence of kernel methods is mainly based on the density and the quality of trial and test points. There are three geometrical quantities associated with X. The *fill distance* of X on $\mathbb{M}$ is defined by

$$h_{X,\mathbb{M}} = \sup_{x \in \mathbb{M}} \min_{1 \leq j \leq N} d_{\mathbb{M}}(\boldsymbol{x}, \boldsymbol{x}_j),$$

where $d_{\mathbb{M}}(\boldsymbol{x}, \boldsymbol{x}_j)$ denotes the geodesic distance between $\boldsymbol{x}$ and $\boldsymbol{x}_j$ on $\mathbb{M}$. The *separation distance* of X on $\mathbb{M}$ is defined by

$$q_{X,\mathbb{M}} = \frac{1}{2} \min_{i \neq j} d_{\mathbb{M}}(\boldsymbol{x}_i, \boldsymbol{x}_j),$$

and finally the mesh ration $\rho_{X,\mathbb{M}}$ of set X is defined by

$$\rho_{X,\mathbb{M}} = \frac{h_{X,\mathbb{M}}}{q_{X,\mathbb{M}}},$$

which measures how uniformly the points are placed on $\mathbb{M}$. When $\rho_{X,\mathbb{M}}$ is close to 1 then the distribution of points is said to be *quasi-uniform*. For $R > 1$, let $\mathcal{X}_R = \mathcal{X}_R(\mathbb{M})$ be the family of all sets of centers X with $\rho_{X,\mathbb{M}} \leq R$; we will say that the family $\mathcal{X}_R$ is R-uniform.

We need a *sampling inequality* (or *zeros theorem* when $u|_X = 0$) to derive an error estimate for the above mentioned meshfree method. Sampling inequalities in Sobolev spaces estimate the W_q^β-norm of a function u by its stronger W_p^σ-norm times certain powers of fill distance h of a set X plus a discrete norm of the function's sampled values at X. In [38,46], a sampling inequality in bounded domains in $\mathbb{R}^d$ has been proved for $\sigma \in \mathbb{R}$, $p \in [1, \infty)$, $q \in [1, \infty]$, $\lfloor \sigma \rfloor > d/p$ if $p > 1$ or $\lfloor \sigma \rfloor \geq d$ if $p = 1$, and for non-negative integer values of β up to $\lfloor \sigma \rfloor - d/p$. In [2] the admissible values of β, σ and p have been enlarged and the following sampling inequality has been derived

$$|u|_{W_q^\beta(\Omega)} \leq C \left(h_{X,\Omega}^{\sigma-\beta-d(1/p-1/q)_+} |u|_{W_p^\sigma(\Omega)} + h_{X,\Omega}^{-\beta} \|u|_X\|_{\ell_\infty} \right) \tag{5.1}$$

where $p, q \in [1, \infty]$, $\sigma \in \mathbb{R}$, $\sigma > d/p$ if $p > 1$ or $\sigma \geq d$ if $p = 1$, and $\beta \in \mathbb{N}_0$ satisfies $0 \leq \beta \leq \lceil \sigma - d(1/p - 1/q)_+ \rceil - 1$. Here $\Omega \subset \mathbb{R}^d$ has a Lipschitz continuous boundary. In [22] (5.1) has been employed on charts to find the following sampling inequality on a k-dimensional submanifold $\mathbb{M}$:

$$|u|_{W_q^\beta(\mathbb{M})} \leq C h_{X,\mathbb{M}}^{\sigma-\beta-k(1/p-1/q)_+} |u|_{W_p^\sigma(\mathbb{M})}, \tag{5.2}$$

where $u|_X = 0$. Here, $p, q \in [1, \infty]$, $\sigma > k/p$ if $p > 1$ or $\sigma \geq k$ if $p = 1$ and $\beta \in \mathbb{N}_0$ with $0 \leq \beta \leq \lceil \sigma - k(1/p - 1/q)_+ \rceil - 1$. In [3] the sampling inequality (5.1) has been generalized for real values of β but excluding the case $q = \infty$.

By applying the strategy of [22] and [27] (the latter concerns the case $\mathbb{M} = \mathbb{S}^{d-1}$), (5.2) can be extended to

$$|u|_{W_q^\beta(\mathbb{M})} \leq C \left(h_{X,\mathbb{M}}^{\sigma-\beta-k(1/p-1/q)_+} |u|_{W_p^\sigma(\mathbb{M})} + h_{X,\mathbb{M}}^{-\beta} \|u|_X\|_{\ell_\infty} \right), \tag{5.3}$$

for well-distributed point set X on $\mathbb{M}$. Although (5.3) will be used in the sequel, we further need a zeros theorem for values of β ranging from zero to σ in the case where both β and σ are real and $p = q = 2$. Fortunately, [45, Theorem 4.6] proves such case for bounded domains in $\mathbb{R}^d$. Again applying the strategy of [22] and using [45, Theorem 4.6] instead of (5.1) we have the following result.

Theorem 5.2 *Let $\mathbb{M}$ be a smooth manifold of dimension k, and let $p, q \in (1, \infty)$ and $\sigma > k/p$. Assume $\beta \in \mathbb{R}$ satisfies $0 \leq \beta \leq \sigma - k(1/p - 1/q)_+$. Also, let $X \subset \mathbb{M}$ be a discrete set with sufficiently small fill distance $h_{X,\mathbb{M}}$. Then we have*

$$|u|_{W_q^\beta(\mathbb{M})} \leq C h_{X,\mathbb{M}}^{\sigma-\beta-k(1/p-1/q)_+} |u|_{W_p^\sigma(\mathbb{M})}, \tag{5.4}$$

provided that $u \in W_p^\sigma(\mathbb{M})$ and $u|_X = 0$.

Noting that, in the all above sampling inequalities the semi-norms can be replaced by full Sobolev norms on the left and right sides.

In the rest of this section, we will show how well L_X approximates $\Delta_{\mathbb{M}}$. We need to define the continuous analogues of discrete differential matrices G_X and L_X. Following [20] we define

$$G_{\mathbb{M}} u := \nabla_{\mathbb{M}} I_\phi u, \quad D_{\mathbb{M}} \boldsymbol{u} = \nabla_{\mathbb{M}} \cdot I_\phi \boldsymbol{u}, \quad L_{\mathbb{M}} u = D_{\mathbb{M}} G_{\mathbb{M}} u,$$

where $I\boldsymbol{u} = (Iu^x, Iu^y, Iu^z)$ is the vector-valued kernel interpolant of $\boldsymbol{u}$. We note that the function $L_{\mathbb{M}} u$ sampled at X is equivalent to associated differential matrix L_X acting on u_X, i.e.

$$(L_{\mathbb{M}} u)_X = L_X u_X. \tag{5.5}$$

Our results below (Theorem 5.4) complete the results of [20, Theorems 1 and 2] for target functions in Sobolev spaces $H^\sigma(\mathbb{M})$ for all real values of σ with $3 < \sigma \leq 2s$. For this purpose, we need to generalize the kernel interpolation error estimate given in [22, Theorem 17].

Theorem 5.3 *Let $\mathbb{M}$ be a smooth k-dimensional submanifold of $\mathbb{R}^d$. Assume $\Phi = \phi(\|\cdot\|_2)$ satisfies (3.4) for $\tau > d/2$, and define $s = \tau - (d-k)/2$. Let $X \subset \mathbb{M}$ be a discrete set having fill distance $h = h_{X,\mathbb{M}}$ sufficiently small and mesh ratio $\rho = \rho_{X,\mathbb{M}}$. Then we have*

$$\|u - I_\phi u\|_{H^\beta(\mathbb{M})} \leq \begin{cases} Ch^{\sigma-\beta}\rho^{s-\sigma}\|u\|_{H^\sigma(\mathbb{M})}, & k/2 < \sigma \leq s, \\ Ch^{\sigma-\beta}\|u\|_{H^\sigma(\mathbb{M})}, & s \leq \sigma \leq 2s, \end{cases} \tag{5.6}$$

for all $u \in H^\sigma(\mathbb{M})$ and $0 \leq \beta \leq s$. Here, both σ and β are real parameters.

Proof The proof of the first estimate for $k/2 < \sigma \leq s$ follows from the proof of [22, Theorem 17] by applying the sampling inequality (5.4) instead of (5.2) for $p = q = 2$. In additions, [22, Corollary 15] concerns the case $\sigma = 2s$. Here we prove the second estimate in (5.6), for $s \leq \sigma \leq 2s$, by using a duality trick as follows: The minimal property of $I_\phi u$ in the native space of ϕ implies $\langle u - I_\phi u, I_\phi u\rangle_{H^s(\mathbb{M})} = 0$ leading to

$$\|u - I_\phi u\|^2_{H^s(\mathbb{M})} = \langle u - I_\phi u, u\rangle_{H^s(\mathbb{M})}.$$

Let $v := u - I_\phi u$. Using the definition of inner products and norms by the Fourier transform (up to a constant factor) we have for any $\alpha \in [0, s]$,

$$\begin{aligned}
\|u - I_\phi u\|^2_{H^s(\mathbb{M})} = \langle u, v\rangle_{H^s(\mathbb{M})} &= \sum_{j=1}^J \langle u_j, v_j\rangle_{H^s(\mathbb{R}^k)} \\
&= \sum_{j=1}^J \int_{\mathbb{R}^k} (1 + \|\omega\|_2^2)^s \widehat{u}_j(\omega)\overline{\widehat{v_j}(\omega)} d\omega \\
&\leq \sum_{j=1}^J \int_{\mathbb{R}^k} (1 + \|\omega\|_2^2)^{s/2+\alpha/2} |\widehat{u}_j(\omega)| (1 + \|\omega\|_2^2)^{s/2-\alpha/2} |\widehat{v}_j(\omega)| d\omega \\
&\leq \sum_{j=1}^J \left(\int_{\mathbb{R}^k} (1 + \|\omega\|_2^2)^{s+\alpha} |\widehat{u}_j(\omega)|^2 d\omega \right)^{1/2} \\
&\quad \times \left(\int_{\mathbb{R}^k} (1 + \|\omega\|_2^2)^{s-\alpha} |\widehat{v}_j(\omega)|^2 d\omega \right)^{1/2} \\
&= \sum_{j=1}^J \|u_j\|_{H^{s+\alpha}(\mathbb{R}^k)} \|v_j\|_{H^{s-\alpha}(\mathbb{R}^k)} \\
&\leq \left(\sum_{j=1}^J \|u_j\|^2_{H^{s+\alpha}(\mathbb{R}^k)} \right)^{1/2} \left(\sum_{j=1}^J \|v_j\|^2_{H^{s-\alpha}(\mathbb{R}^k)} \right)^{1/2} \\
&= \|u\|_{H^{s+\alpha}(\mathbb{M})} \|v\|_{H^{s-\alpha}(\mathbb{M})},
\end{aligned}$$

where $u_j = \pi_j(u)$ and $v_j = \pi_j(v)$ are defined in Definition 5.1. The Cauchy-Schwartz inequalities in $L^2(\mathbb{R}^k)$ and $\mathbb{R}^J$ have been used in the fourth and seventh lines, respectively.

To bound the last term, an application of inequality (5.4) for $p = q = 2$ yields

$$\begin{aligned}\|v\|_{H^{s-\alpha}(\mathbb{M})} &= \|u - I_\phi u\|_{H^{s-\alpha}(\mathbb{M})} \\ &\le Ch^\alpha \|u - I_\phi u\|_{H^s(\mathbb{M})},\end{aligned}$$

because $u - I_\phi u$ is zero on X. Setting $\alpha = \sigma - s$ gives

$$\|u - I_\phi u\|_{H^s(\mathbb{M})} \le Ch^{\sigma-s}\|u\|_{H^\sigma(\mathbb{M})}, \quad s \le \sigma \le 2s.$$

Another application of (5.4) for $p = q = 2$ then leads to the second error bound in (5.6). □

With this, we can prove the following result.

Theorem 5.4 *Let $\mathbb{M}$ be a smooth 2-dimensional submanifold of $\mathbb{R}^3$. Assume that $\Phi = \phi(\|\cdot\|_2)$ satisfies (3.4) with $\tau > 3/2 + 2$ and $s = \tau - 1/2$. Let $X \subset \mathbb{M}$ be a discrete set having fill distance $h = h_{X,\mathbb{M}}$ sufficiently small and mesh ratio $\rho = \rho_{X,\mathbb{M}}$. Then*

$$\|L_{\mathbb{M}}u - \Delta_{\mathbb{M}}u\|_{L_q(\mathbb{M})} \le \begin{cases} Ch^{\sigma-2-2(1/2-1/q)_+}\rho^{2(s-\sigma)+1}\|u\|_{H^\sigma(\mathbb{M})}, & 3 < \sigma \le s, \\ Ch^{\sigma-2-2(1/2-1/q)_+}\rho\|u\|_{H^\sigma(\mathbb{M})}, & s \le \sigma \le 2s, \end{cases} \tag{5.7}$$

for all $u \in H^\sigma(\mathbb{M})$ and $1 \le q \le \infty$.

Proof The estimate for $3 < \sigma \le s$ is exactly that of [20, Theorem 1]. Theorem 2 of this reference concerns the error bound for functions at least twice smoother than those in the native space of Φ. Here, we complete this for functions in $H^\sigma(\mathbb{M})$, where $s \le \sigma \le 2s$. The argument is mainly based on the error estimate (5.6) for $s \le \sigma \le 2s$ for pure interpolation problem. First, since $s > 3$ we have $\lceil s - 2(1/2 - 1/q)_+\rceil - 1 \ge \lceil s - 1\rceil - 1 = \lceil s\rceil - 2 \ge 4 - 2 = 2$. Thus, from sampling inequality (5.3) together with error bound (5.6) we obtain

$$\begin{aligned}\|u - I_\phi u\|_{W_q^2(\mathbb{M})} &\le Ch^{s-2-2(1/2-1/q)_+}\|u - I_\phi u\|_{H^s(\mathbb{M})} \\ &\le Ch^{\sigma-2-2(1/2-1/q)_+}\|u\|_{H^\sigma(\mathbb{M})},\end{aligned} \tag{5.8}$$

for $s \le \sigma \le 2s$. Next, we can write

$$\|\Delta_{\mathbb{M}}u - L_{\mathbb{M}}u\|_{L_q(\mathbb{M})} \le \|\Delta_{\mathbb{M}}u - \Delta_{\mathbb{M}}I_\phi u\|_{L_q(\mathbb{M})} + \|L_{\mathbb{M}}u - \Delta_{\mathbb{M}}I_\phi u\|_{L_q(\mathbb{M})}. \tag{5.9}$$

The first term on the right hand side of (5.9) can be estimated via (5.8) by

$$\begin{aligned}\|\Delta_{\mathbb{M}}u - \Delta_{\mathbb{M}}I_\phi u\|_{L_q(\mathbb{M})} &\le C\|u - I_\phi u\|_{W_q^2(\mathbb{M})} \\ &\le Ch^{\sigma-2-2(1/2-1/q)_+}\|u\|_{H^\sigma(\mathbb{M})},\end{aligned}$$

for all $s \le \sigma \le 2s$. We note that $I_\phi u \in H^\nu(\mathbb{M})$ for all $\nu < 2s - 1$, $\nabla_{\mathbb{M}}I_\phi u \in \mathbf{H}^\nu(\mathbb{M})$ for all $\nu < 2s - 2$ and $\nabla_{\mathbb{M}}u \in \mathbf{H}^{s-1}(\mathbb{M})$ for $u \in H^\sigma(\mathbb{M})$ for all $\sigma \ge s$. Here $\mathbf{H}^\nu(\mathbb{M}) = (H^\nu(\mathbb{M}))^3$. With these and from the details of the proof of [20, Theorem 2], the second term on the right hand side of (5.9) can be estimated by

$$\begin{aligned}\|L_{\mathbb{M}}u - \Delta_{\mathbb{M}}I_\phi u\|_{L_q(\mathbb{M})} \le Ch^{s-2-2(1/2-1/q)_+}\Big[&(\rho+1)\|\nabla_{\mathbb{M}}u - \nabla_{\mathbb{M}}I_\phi u\|_{\mathbf{H}^{s-1}(\mathbb{M})} \\ &+ \|I_\phi(\nabla_{\mathbb{M}}u) - \nabla_{\mathbb{M}}u\|_{\mathbf{H}^{s-1}(\mathbb{M})}\Big].\end{aligned}$$

The first norm on the right hand side in the above inequality can be bounded via (5.6) as

$$\|\nabla_{\mathbb{M}}u - \nabla_{\mathbb{M}}I_\phi u\|_{\mathbf{H}^{s-1}(\mathbb{M})} \le C\|u - I_\phi u\|_{H^s(\mathbb{M})}$$

$$\leq Ch^{\sigma-s}\|u\|_{H^\sigma(\mathbb{M})},$$

which is valid for $s \leq \sigma \leq 2s$. The second norm can be treated as

$$\begin{aligned}\|I_\phi(\nabla_{\mathbb{M}}u) - \nabla_{\mathbb{M}}u\|_{\mathbf{H}^{s-1}(\mathbb{M})} &\leq Ch^{(\sigma-1)-(s-1)}\|\nabla_{\mathbb{M}}u\|_{\mathbf{H}^{\sigma-1}(\mathbb{M})}\\ &\leq Ch^{\sigma-s}\|u\|_{H^\sigma(\mathbb{M})},\end{aligned}$$

for $s \leq \sigma \leq 2s$. Summarizing all, we finally get

$$\|\Delta_{\mathbb{M}}u - L_{\mathbb{M}}u\|_{L_q(\mathbb{M})} \leq C(\rho+2)h^{\sigma-2-2(1/2-1/q)_+}\|u\|_{H^\sigma(\mathbb{M})},$$

which completes the proof. □

The error estimate (5.7) can be easily generalized for the case where $\mathbb{M}$ is a k-dimensional submanifold of $\mathbb{R}^d$.

5.1 Stability Analysis

According to (4.1), in order to prevent the instability in numerical solution U_X^{n*}, time step Δt and fill distance $h_{X,\mathbb{M}}$ might be chosen such that $\rho(I_N + \Delta t L_X) \leqslant 1$, where $\rho(A)$ is the spectral radius of matrix A, and I_N is the identity matrix of size N. If λ is any eigenvalue of L_X this requires $\mathrm{Re}(\lambda) < 0$ and $\Delta t \leq 2|\mathrm{Re}(\lambda)|/|\lambda|^2$. Numerous experimental results in [20] show that if the surface $\mathbb{M}$ is well-discretized, i.e., for sufficiently small values of $h_{X,\mathbb{M}}$, all eigenvalues of L_X lie in the left half plane. In additions, the imaginary part is much smaller than the real part in magnitude. No analytical proof is yet available for this assertion. Thus, following [20] and our own observations, we conjecture that:

Conjecture 1 *All diagonal elements of L_X are negative and if the surface $\mathbb{M}$ is well-discretized then all eigenvalues λ of L_X lie in the left half plane. Moreover, $|\lambda| = \mathcal{O}(|\mathrm{Re}(\lambda)|)$.*

However, for the second requirement $\Delta t \leq 2|\mathrm{Re}(\lambda)|/|\lambda|^2$ which, by accepting Conjecture 1, is now become $\Delta t \leq c/\rho(L_X)$, for a sufficiently small constant c, we estimate $\rho(L_X)$ in terms of fill distance $h_{X,\mathbb{M}}$.

Theorem 5.5 *Assume that L_X is formed via $X = \{\boldsymbol{x}_1, \ldots, \boldsymbol{x}_N\} \in \mathcal{X}_R$ with sufficiently small fill distance $h = h_{X,\mathbb{M}}$, and assume that the kernel $\Phi = \phi(\|\cdot\|_2)$ satisfies (3.4) for $\tau > 3/2 + 2$. Then*

$$\rho(L_X) \leq \|L_X\|_\infty \leq Ch^{-2}, \tag{5.10}$$

where $\rho(L_X)$ is the spectral radius of matrix L_X.

Proof The first inequality in (5.10) is an elementary result in linear algebra. For the second inequality suppose that $\boldsymbol{c} \in \mathbb{R}^N \backslash \{0\}$ is given. For a $\sigma \in \mathbb{R}$ with $3 < \sigma \leqslant 2s$, $s = \tau - 1/2$, choose a function $v \in H^\sigma(\mathbb{M})$ such that $v(\boldsymbol{x}_k) = \boldsymbol{c}_k$ for $k = 1, 2, \ldots, N$. (For example, the ϕ-interpolant of $\boldsymbol{c}_k$-values can be chosen. In this case, σ might be any real number with $3 < \sigma < 2s - 1$). According to (5.5)

$$L_X\boldsymbol{c} = (L_{\mathbb{M}}v)_X.$$

Using this and by applying Theorem 5.4 and sampling inequality (5.3) and using the assumption on quasi-uniformity, we have

$$\|L_X\boldsymbol{c}\|_{\ell_\infty} \leqslant \|L_{\mathbb{M}}v\|_{L_\infty(\mathbb{M})}$$

$$\begin{aligned}
&\leqslant \|\Delta_{\mathbb{M}} v\|_{L_\infty(\mathbb{M})} + \|\Delta_{\mathbb{M}} v - L_{\mathbb{M}} v\|_{L_\infty(\mathbb{M})} \\
&\leqslant \|v\|_{W^2_\infty(\mathbb{M})} + Ch^{\sigma-3}\|v\|_{H^\sigma(\mathbb{M})} \\
&\leqslant Ch^{\sigma-3}\|v\|_{H^\sigma(\mathbb{M})} + Ch^{-2}\|v_X\|_{\ell_\infty}.
\end{aligned}$$

Thus for sufficiently small values of h and using the fact that $v_X = \boldsymbol{c}$ we have $\|L_X \boldsymbol{c}\|_{\ell_\infty} \leq Ch^{-2}\|\boldsymbol{c}\|_{\ell_\infty}$ which leads to the desired bound. □

Corollary 1 *Accepting Conjecture 1, the uniform stability condition for Eq. (4.1) is*

$$\Delta t = ch^2_{X,\mathbb{M}}, \tag{5.11}$$

where c is a sufficiently small constant.

So far we have used the notation u^n, $n \geq 0$, as an approximation for $u(\cdot, t_n)$ which is a function continuous in $\boldsymbol{x}$ but discrete in t. The notation $U^n_X \in \mathbb{R}^N$ has been also denoted for the approximate solution of full-discrete Eqs. (4.1) and (4.2). From here on, the notation $u^n_X \in \mathbb{R}^N$ will be used when u^n is sampled at set point X.

Assume that S_L and S_N represent the linear and the nonlinear operators in (2.4) and (2.5), respectively, such that

$$u^{n+1} = S_N S_L u^n, \quad n = 0, 1, \ldots . \tag{5.12}$$

The discrete analogues of these operators are denoted by S^X_L and S^X_N leading to a reformulation of (4.1) and (4.2) as below

$$U^{n+1}_X = S^X_N S^X_L U^n_X, \quad n = 0, 1, \ldots . \tag{5.13}$$

Since the exact time integration solution has been applied for the nonlinear part, we have

$$(S_N u^n)_X = S^X_N u^n_X \tag{5.14}$$

for all continuous functions u^n. Now, the following lemmas concern the stability of the approximate solution U^{n+1}_X.

Lemma 5.6 *Under the assumptions of Theorem 5.5 and Corollary 1, we have*

$$\|U^{n*}_X\|_{\ell_\infty} = \|S^X_L U^n_X\|_{\ell_\infty} \leq \|U^n_X\|_{\ell_\infty},$$

provided that $2\Delta t \geq \left(\min_{1\leq k\leq N} |\ell_{kk}|\right)^{-1}$ *where* ℓ_{kk} *are diagonal elements of* L_X.

Proof Using the last assumption and the fact that L_X has negative diagonal elements, we have $\|S^X_L\|_\infty = \|I_N + \Delta t L_X\|_\infty \leq \Delta t \|L_X\|_\infty$. From Theorem 5.5 and using the stability condition (5.11) we have $\Delta t \|L_X\|_\infty \leq C\Delta t h^{-2}_{X,\mathbb{M}} \leq 1$ for appropriate choices of Δt. This leads to the desired bound. □

Many experimental results show $|\ell_{kk}|$ behave like $h^{-2}_{X,\mathbb{M}}$ which suggests some accessible values for Δt in Lemma 5.6. However, experiments show that this restriction on Δt is not actually required. Thus, a new analysis which ignores this restriction will be welcome in future studies.

Lemma 5.7 *Under the assumptions of Theorem 5.5, we have*

$$\|U^{n+1}_X\|_{\ell_\infty} \leq e^{\frac{T}{E^2}} \|U^0_X\|_{\ell_\infty},$$

provided that (5.11) holds.

Proof First, for $n \geq 0$ and $k = 1, \ldots, N$ we have

$$\left| \left(U_X^{n+1}\right)_k \right| = \left| \frac{\left(U_X^{n*}\right)_k}{\sqrt{e^{-\frac{2\Delta t}{E^2}} + \left(1 - e^{-\frac{2\Delta t}{E^2}}\right)\left(U_X^{n*}\right)_k^2}} \right| \leq e^{\frac{\Delta t}{E^2}} \left| \left(U_X^{n*}\right)_k \right|,$$

leading to

$$\|U_X^{n+1}\|_{\ell_\infty} \leq e^{\frac{\Delta t}{E^2}} \|U_X^{n*}\|_{\ell_\infty}.$$

Then Lemma 5.6 and a recursive application for $n \geq 0$ yield the desired bound. □

5.2 Convergence Analysis

The convergence analysis at nodal points X is given here. First, we prove the following lemma.

Lemma 5.8 *Let $\mathbb{M}$ be a smooth 2-dimensional submanifold of $\mathbb{R}^3$. Assume that Φ satisfies (3.4) for $\tau > 3/2 + 2$ and let $s = \tau - 1/2$. For $n \geq 0$ suppose that $u^n \in H^\sigma(\mathbb{M})$ for $3 < \sigma \leq 2s$. For $X \in \mathcal{X}_R$ with sufficiently small fill distance $h = h_{X,\mathbb{M}}$ we have*

$$\|(S_L u^n)_X - S_L^X u_X^n\|_{\ell_\infty} \leqslant C \Delta t \, h^{\sigma-3} \|u^n\|_{H^\sigma(\mathbb{M})}.$$

Proof Remember that $S_L = I + \Delta t \Delta_{\mathbb{M}}$ and $S_L^X = I_N + \Delta t L_X$, where I is the identity operator and I_N is the N-by-N identity matrix. We can write

$$\begin{aligned} \|(S_L u^n)_X - S_L^X u_X^n\|_{\ell_\infty} &= \|u_X^n + \Delta t(\Delta_{\mathbb{M}} u^n)_X - u_X^n - \Delta t L_X u_X^n\|_{\ell_\infty} \\ &= \Delta t \|(\Delta_{\mathbb{M}} u^n)_X - L_X u_X^n\|_{\ell_\infty} \\ &\leq \Delta t \|\Delta_{\mathbb{M}} u^n - L_{\mathbb{M}} u^n\|_{L_\infty(\mathbb{M})} \\ &\leq C \Delta t \, h^{\sigma-3} \|u^n\|_{H^\sigma(\mathbb{M})}, \end{aligned}$$

where in the third and in the last lines we have used Eq. (5.5) and Theorem 5.4, respectively. □

Theorem 5.9 *Under the assumptions of Lemma 5.8 we have*

$$\|u_X(t_{n+1}) - U_X^{n+1}\|_{\ell_\infty} \leqslant C(\|u^0\|_{H^2(\mathbb{M})})\Delta t + C h^{\sigma-3} \max_{0 \leq k \leq n} \|u^k\|_{H^\sigma(\mathbb{M})}.$$

provided that the stability condition (5.11) holds.

Proof First, by adding and subtracting u_X^{n+1}, we have

$$\|u_X(t_{n+1}) - U_X^{n+1}\|_{\ell_\infty} \leq \|u_X(t_{n+1}) - u_X^{n+1}\|_{\ell_\infty} + \|u_X^{n+1} - U_X^{n+1}\|_{\ell_\infty}.$$

The first term in the right hand side is the total error of the time difference approximation which itself contains the error of splitting (1.1) into (2.2) and the error of discretizations (2.4)–(2.5). According to [12] and [6, Theorem 4.1] both errors are of order Δt. More precisely, we have

$$\|u_X(t_{n+1}) - u_X^{n+1}\|_{\ell_\infty} \leqslant C(\|u^0\|_{H^2(\mathbb{M})})\Delta t,$$

where u^0 is the initial data function. The second term can be treated as

$$\begin{aligned}\|u_X^{n+1} - U_X^{n+1}\|_{\ell_\infty} &= \|(S_N S_L u^n)_X - S_N^X S_L^X U_X^n\|_{\ell_\infty} \\ &\le \|(S_N S_L u^n)_X - S_N^X (S_L u_X^n)_X\|_{\ell_\infty} + \|S_N^X (S_L u^n)_X - S_N^X S_L^X U_X^n\|_{\ell_\infty} \\ &\le 0 + e^{\frac{\Delta t}{E^2}} \|(S_L u^n)_X - S_L^X U_X^n\|_{\ell_\infty},\end{aligned}$$

where in the last line, Eq. (5.14) and Lemma 5.7 are used. To bound the right hand side, we have

$$\begin{aligned}\|(S_L u^n)_X - S_L^X U_X^n\|_{\ell_\infty} &\le \|(S_L u^n)_X - S_L^X u_X^n\|_{\ell_\infty} + \|S_L^X u_X^n - S_L^X U_X^n\|_{\ell_\infty} \\ &\le C \Delta t\, h^{\sigma-3} \|u^n\|_{H^\sigma(\mathbb{M})} + \|u_X^n - U_X^n\|_{\ell_\infty},\end{aligned}$$

where Lemmas 5.6 and 5.8 and the assumption on quasi-uniformity have been used. Consequently, we have

$$\|u_X^{n+1} - U_X^{n+1}\|_{\ell_\infty} \le e^{\frac{\Delta t}{E^2}} \left(C \Delta t\, h^{\sigma-3} \|u^n\|_{H^\sigma(\mathbb{M})} + \|u_X^n - U_X^n\|_{\ell_\infty} \right).$$

By induction and using the fact that $u_X^0 = U_X^0$ we get

$$\begin{aligned}\|u_X^{n+1} - U_X^{n+1}\|_{\ell_\infty} &\le C \Delta t\, h^{\sigma-3} \max_{0\le k\le n} \|u^k\|_{H^\sigma(\mathbb{M})} \left\{ \sum_{k=1}^{n+1} e^{\frac{k\Delta t}{E^2}} \right\} \\ &= C \Delta t\, h^{\sigma-3} \max_{0\le k\le n} \|u^k\|_{H^\sigma(\mathbb{M})} \left\{ e^{\frac{\Delta t}{E^2}} \left(e^{\frac{t_{n+1}}{E^2}} - 1 \right) \frac{1}{e^{\frac{\Delta t}{E^2}} - 1} \right\} \\ &\le C h^{\sigma-3} \max_{0\le k\le n} \|u^k\|_{H^\sigma(\mathbb{M})},\end{aligned}$$

where in the last line the inequality $1/(e^x - 1) \le 1/x$ for $x > 0$ has been used. Summarizing all, we get the desired bound. □

6 Numerical Simulations

This section is devoted to some numerical simulations using the proposed method for the AC model (1.1). In numerical simulations the sphere, the torus and the red blood cell are used as surfaces. These 2-dimensional manifolds are defined as below:

$$\begin{aligned}\mathbb{M} &= \left\{ (x, y, z) \in \mathbb{R}^3 : x^2 + y^2 + z^2 = r_0^2 \right\}, \\ \mathbb{M} &= \left\{ (x, y, z) \in \mathbb{R}^3 : \left(c_1 - \sqrt{x^2 + y^2} \right)^2 + z^2 = r_1^2 \right\}, \\ \mathbb{M} &= \left\{ (x, y, z) \in \mathbb{R}^3 : \left(1 - \frac{x^2 + y^2}{r_2^2} \right) \left(c_0 + c_2 \left(\frac{x^2 + y^2}{r_2^2} \right) + c_4 \left(\frac{x^2 + y^2}{r_2^2} \right)^2 \right)^2 - 4z^2 = 0 \right\}.\end{aligned}$$

For problems in Sects. 6.1 and 6.2 we set $r_0 = 1, r_1 = 0.3, r_2 = 3.91/3.39, c_0 = 0.81/3.39, c_1 = 0.7, c_2 = 7.83/3.39, c_4 = -4.39/3.39$, while for that in Sect. 6.3 we set $r_0 = 0.3$, $r_1 = 1/16, r_2 = 3.39/0.3, c_1 = 0.4$ with the same c_0, c_2 and c_4 as before. The unit sphere, the torus and the red blood cell will be denoted by $\mathbb{S}^2$, $\mathbb{T}^2$ and $\mathbb{B}^2$, respectively.

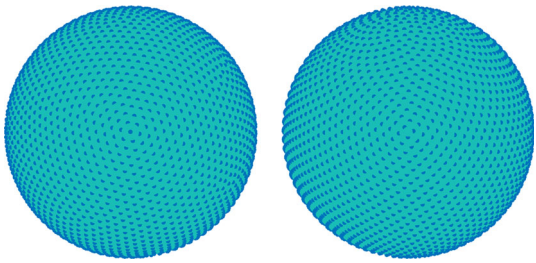

Fig. 1 PTS points (left) and ME points (right) on $\mathbb{S}^2$

The Matérn kernel (3.5) with $\nu = 5$ is employed as a trial kernel. This kernel satisfies (3.4) with $\tau = 5$ which means that it has $H^5(\mathbb{R}^3)$ as its native space [16]. Thus, the native space of its restriction to the above 2-dimensional submanifolds $\mathbb{M}$ is $H^{4.5}(\mathbb{M})$.

In experiments the shape parameter $\varepsilon = 10$ is used. The numerical order of convergence in spatial and time domains is computed via the following formula

$$\frac{\log\left(\frac{e_{\text{old}}}{e_{\text{new}}}\right)}{\log\left(\frac{h_{\text{old}}}{h_{\text{new}}}\right)},$$

where e and h represent the numerical error and the fill distance, respectively. The errors are measured in $\ell_\infty(X)$-norm where X is a set of scattered points on $\mathbb{M}$. The numerical order of growth of $\rho(L_X)$ is calculated similarly.

6.1 Test Problems

To show the order of convergence of the proposed scheme, we consider Eq. (1.1) with exact solution

$$u(x, y, z, t) = \tanh(x + y + z - t), \tag{6.1}$$

for $(x, y, z) \in \mathbb{S}^2, t \geq 0$ and $E = 1$. The right hand side function f is calculated accordingly. The minimum energy (ME) and the phyllotaxis spiral (PTS) points are used in this example. These sets of points are quasi-uniform and their fill distance h is of order $N^{-1/2}$. In Fig. 1 a set of 2601 ME and a set of 2601 PTS points are shown. In Fig. 2, the ℓ_∞ errors and the orders of convergence in the spatial domain (in terms of h) have been shown for ME and PTS points with $\Delta t = 10^{-8}$ at time $T = 0.0001$. Theorem 5.4 predicts the rate $h^{2s-3} = h^6$ for smooth solutions. However, numerical results show a better order of convergence. In Fig. 3, the errors and the numerical orders of convergence with respect to the time discretization are plotted for both ME and PTS points at different time levels. The theoretical order $(\Delta t)^1$ is confirmed for both cases. In "Appendix", the MATLAB code of this test problem is given.

Now, we consider the AC equation on torus $\mathbb{T}^2$ with the same exact solution (6.1) and $E = 1$. To generate $(\sqrt{n} - 1)^2$ points on $\mathbb{T}^2$, we first consider the natural parameterization for $\mathbb{T}^2$ as follows:

$$x = (c_1 + r_1\cos(\theta))\cos(\varphi), \quad y = (c_1 + r_1\cos(\theta))\cos(\varphi), \quad z = r_1\sin(\theta), \quad 0 \leq \theta, \varphi \leq 2\pi.$$

In the second round, we have considered $\sqrt{n} - 1$ equally spaced angles $w \in [0, 2\pi)$ and $v \in [0, 2\pi)$, and then take a direct product to gain $(\sqrt{n} - 1)^2$ points [21]. Figure 4 shows a set of gridded points on $\mathbb{T}^2$. In Fig. 5, the errors and the orders of convergence in both spatial and time domains are drawn. The numerical order in spatial domain is much better than the

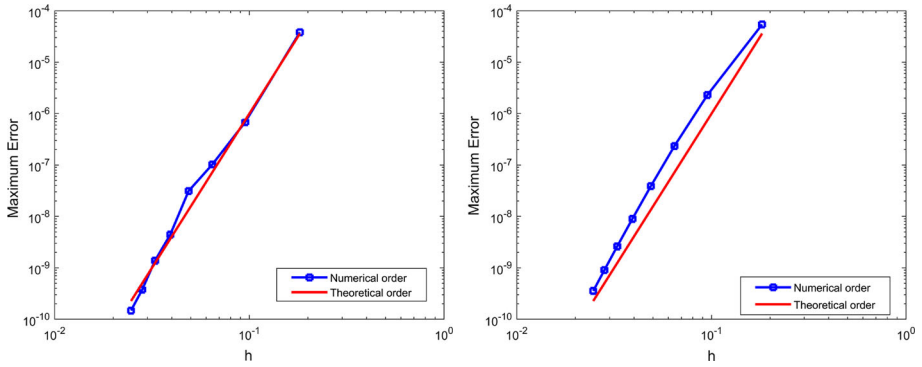

Fig. 2 The maximum errors and orders of convergence in terms of h using ME points (left) and PTS points (right)

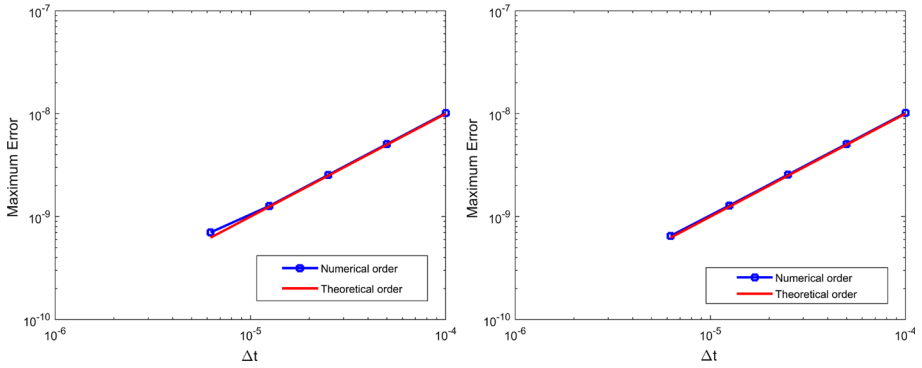

Fig. 3 The maximum errors and orders of convergence on $\mathbb{S}^2$ in terms of Δt using ME points (left) and PTS points (right)

Fig. 4 Gridded points on $\mathbb{T}^2$

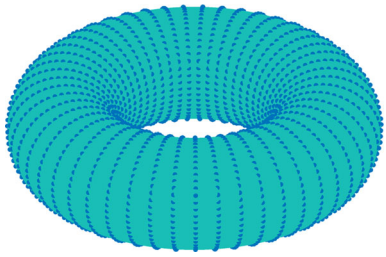

theoretical order h^6. We observe the same phenomenon in [21] which has been related to a kind of supperconvergence at collocation points. This requires more in-depth study in a future work.

Table 1 shows the order of growth of $\rho(L_X)$ for different values of N. Results show that it grows approximately by h^{-2}, which confirm the theoretical bound (5.10).

Here, we support Conjecture 1 in Figs. 6, 7 and 8 where the eigenvalues of differentiation matrix L_X are plotted for three considered manifolds at different number of collocation points. We observe that, for fine discretizations, all eigenvalues lie in the left half plane, and the magnitude of them is of order of the magnitude of their real parts.

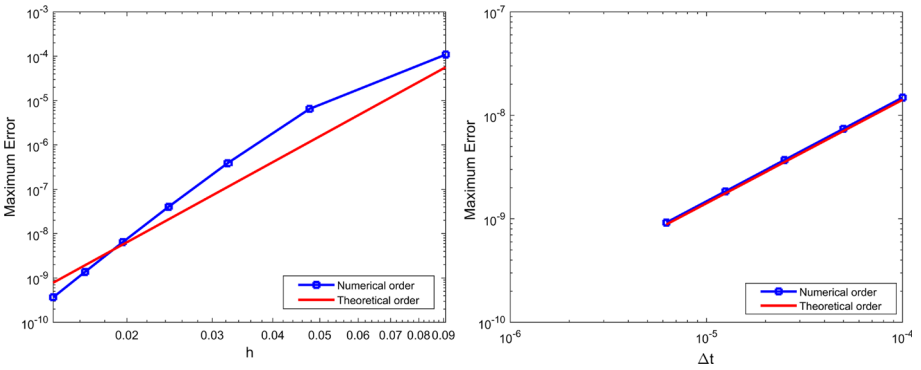

Fig. 5 The maximum errors and orders of convergence on torus in terms of h (left) and Δt (right)

Table 1 The numerical order of growth of $\rho(L_X)$ for different set points X

N	ME points $\rho(L_X)$	orders	PTS points $\rho(L_X)$	orders
121	3.84e+1	–	3.94e+1	–
484	2.44e+2	− 2.67	2.56e+2	− 2.70
1936	1.07e+3	− 2.13	1.19e+3	− 2.22
7744	4.38e+3	− 2.04	5.04e+3	− 2.08

Fig. 6 Eigenvalues of L_X on the unit sphere and PTS points

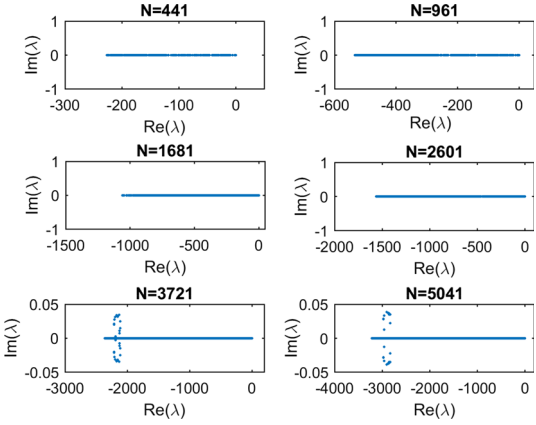

6.2 Motion by Mean Curvature on Surfaces

As first example, consider Eq. (1.1) on $\mathbb{S}^2$ with the following initial condition [11].

$$u(x, y, z, 0) = \tanh\left(\frac{\sqrt{x^2 + y^2} - z}{\sqrt{2}E}\right), \quad (x, y, z) \in \mathbb{S}^2, \tag{6.2}$$

for $E = 0.1$. This test is an example of the well-known motion by mean curvature on the unit sphere [11]. According to (5.11), to guarantee the stability of time discretization, and to have a comparison with the results of [11], we set $\Delta t = 0.416h^2$. Figure 9 shows the numerical solution at $t = 800\Delta t$ and $t = 1600\Delta t$ with $N = 2601$ ME points. The plots for PTS points

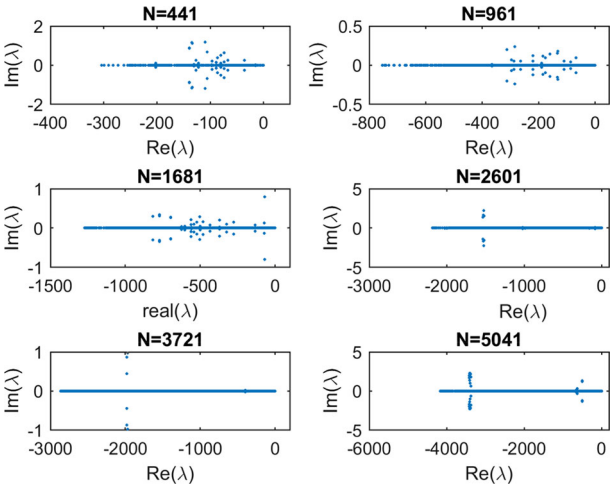

Fig. 7 Eigenvalues of L_X on the red blood cell and PTS points

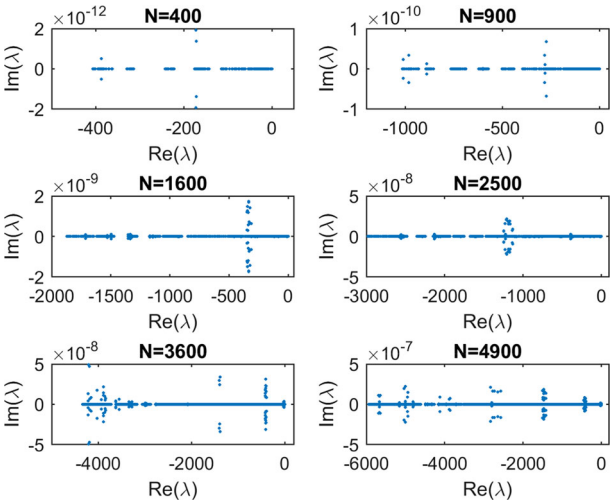

Fig. 8 Eigenvalues of L_X on the torus and gridded points

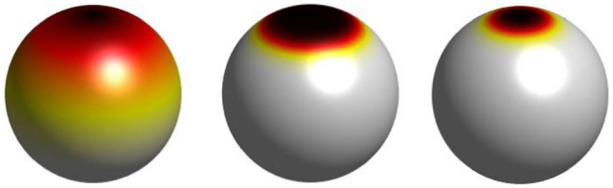

Fig. 9 Motion by mean curvature on $\mathbb{S}^2$ with initial condition (6.2)

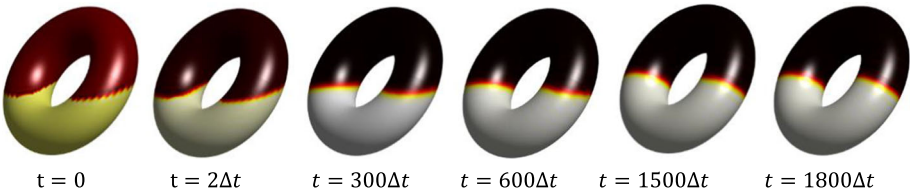

Fig. 10 Motion by mean curvature on $\mathbb{T}^2$ with initial condition (6.3)

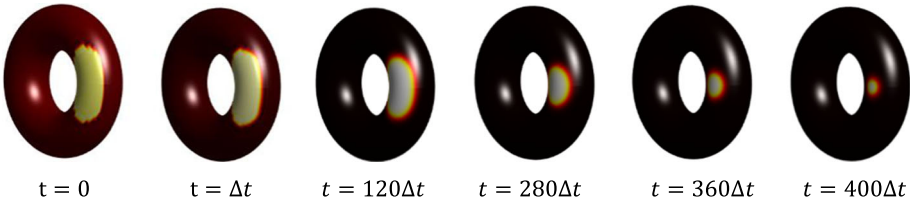

Fig. 11 Motion by mean curvature on $\mathbb{T}^2$ with initial condition (6.4)

which are not shown here are the same. These results are in good agreement with those given in [11].

In the second example, we consider Eq. (1.1) on $\mathbb{T}^2$ with the following initial condition [11].

$$u(x, y, z, 0) = \begin{cases} +1, \ \sqrt{x^2 + z^2} < 1.2 \ \ \& \ \ y + z > 0.1, \\ -1, \ \text{otherwise} \end{cases} \tag{6.3}$$

Numerical results are obtained for $E = 0.0384$, $\Delta t = 1.05h^2$, 6561 gridded points, and depicted in Fig. 10 at $t = 2\Delta t$, $t = 300\Delta t$, $t = 600\Delta t$, $t = 1500\Delta t$ and $t = 1800\Delta t$. Our results are in good agreement with those given in [11].

In the third example, we consider Eq. (1.1) on $\mathbb{T}^2$ and on $\mathbb{B}^2$ with the following initial condition [11]:

$$u(x, y, z, 0) = \begin{cases} +1, \ \sqrt{(x - 0.7)^2 + 0.25y^2} < 0.25 \ \ \& \ \ z > 0, \\ -1, \ \text{otherwise.} \end{cases} \tag{6.4}$$

Numerical solutions are obtained on $\mathbb{T}^2$ for same parameters as in the second example, but given in time levels $t = 120\Delta t$, $t = 280\Delta t$, $t = 360\Delta t$, $t = 400\Delta t$ and $t = 600\Delta t$ in Fig. 11. The results on $\mathbb{B}^2$ are obtained with $N = 6561$ ME points (see Fig. 12) and depicted in Fig. 13. According to the results here and those in [11], the motion by mean curvature can be described as the interface approaches a circle before disappearing, when the steady state is approached.

In the fourth example, we consider Eq. (1.1) on $\mathbb{T}^2$ with the following initial condition [11]:

$$u(x, y, z, 0) = \begin{cases} +1, \ \sqrt{x^2 + y^2} < 0.9 \ \& \ z > 0, \\ +1, \ \sqrt{x^2 + y^2} > 0.7 \ \& \ z < 0, \\ -1, \ \text{otherwise.} \end{cases} \tag{6.5}$$

Numerical solutions are obtained for the same values of numerical parameters as in the second example, but given at time levels $t = \Delta t$, $t = 1500\Delta t$, $t = 2100\Delta t$, $t = 5700\Delta t$

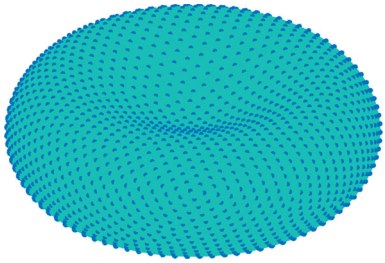

Fig. 12 ME points on red blood cell $\mathbb{B}^2$

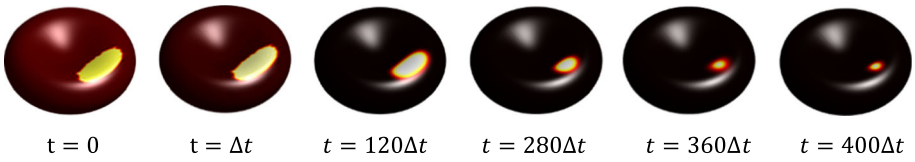

Fig. 13 Motion by mean curvature on red blood cell $\mathbb{B}^2$ with initial condition (6.4)

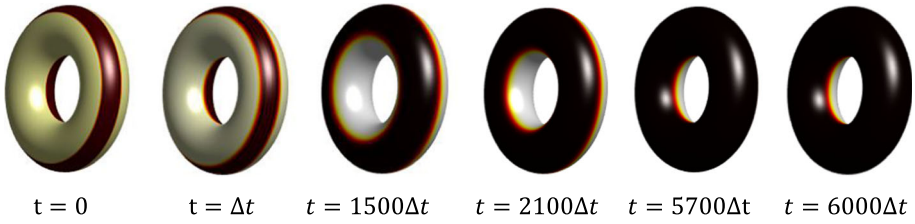

Fig. 14 Motion by mean curvature on torus $\mathbb{T}^2$ with initial condition (6.5)

and $t = 6000\Delta t$ in Fig. 14. Results are in good agreement with [11]. By increasing time, the interfaces shrink by mean curvature, and it reaches to the steady state solution.

6.3 Phase Ordering on Surfaces

In this example, we consider Eq. (1.1) on sphere, torus and red blood cell surfaces with the following initial condition [48]:

$$u(x, y, z, 0) = 0.01 \cdot \text{rand}(x, y, z),$$

where $\text{rand}(x, y, z)$ denotes for a uniformly distributed random number between -1 and 1. This example shows the phase ordering on surfaces which can be observed in ranging from nonequilibrium statistical physics and hydrodynamic theories to cell biology [11]. We set $E = 0.02$ and $\Delta t = 10^{-5}$. In Figs. 15 and 16 the processes of phase separation at times $t = 0.005$, $t = 0.025$ and $t = 0.05$ are shown with $N = 2601$ PTS points on sphere and torus, respectively. These numerical simulations can be verified by the analogous results in [48].

In additions, we obtain the numerical solution with $N = 3721$ ME points on the red blood cell. Figure 17 illustrates the phase separation at times $t = 0.005$, $t = 0.025$ and $t = 0.05$.

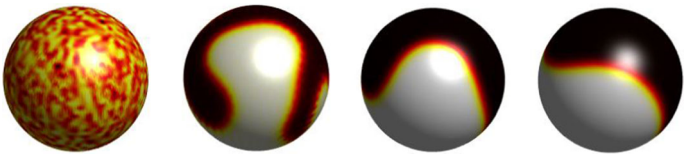

Fig. 15 Phase separation on sphere with a random initial condition

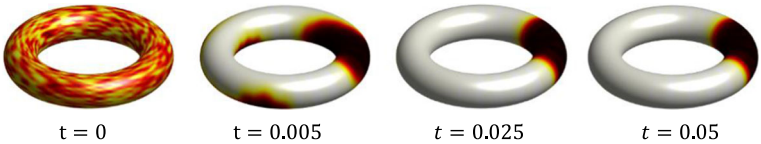

Fig. 16 Phase separation on torus with a random initial condition

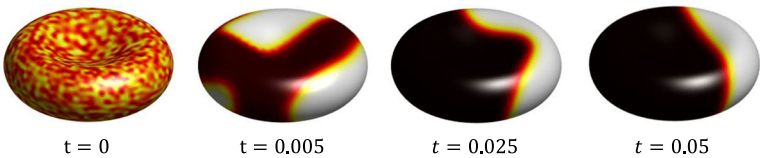

Fig. 17 Phase separation on red blood cell with a random initial condition

7 Conclusion

A numerical solution for the nonlinear time-dependent Allen–Cahn equation on surfaces was obtained using a kernel collocation method in combination with an explicit time splitting algorithm. The convergence analysis of the method was given for functions in appropriate Sobolev spaces defined on surfaces. Some numerical simulations on spheres, toruses and red blood cells were performed to confirm the capability of the presented method.

Acknowledgements The second author was in part supported by a Grant from IPM, No. 96650427. The authors are very grateful to reviewers for carefully reading this paper and for their comments and suggestions which have improved the paper.

Appendix

Here, we provide a sample MATLAB code for simulating the Allen–Cahn equation on the unit sphere. Parts related to the approximation of the Laplace–Beltrami operator are borrowed from [20]. The subroutine for generating the minimum energy points should be provided by user.

```
%% Exact solution u and right-hand side function f
Uexact = @(x,y,z,t) -tanh(-x-y-z+t);
f = @(x,y,z,t,E) -1+tanh(-x-y-z+t).^2+(4*((x.^2+(-y-z).*x+y.^2+z.^2-y.*z).*...
    tanh(-(x+y+z)./sqrt(x.^2+y.^2+z.^2)+t)-(1/2)*sqrt(x.^2+y.^2+z.^2).*...
    (x+y+z))).*(tanh(-(x+y+z)./sqrt(x.^2+y.^2+z.^2)+t)+1).*(tanh(-(x+y+z)...
    ./sqrt(x.^2+y.^2+z.^2)+t)-1)./(x.^2+y.^2+z.^2).^2+(-tanh(-x-y-z+t).^3 ...
    +tanh(-x-y-z+t))/E^2;
%% Matern RBF
phi = @(r,e) exp(-e*r).*(15+15*e*r+6*(e*r).^2+(e*r).^3);
dphi = @(r,e)  -e^2*exp(-e*r).*((e*r).^2+3*e*r+3);
%% Minimum energy points on the unit sphere
N=2601;          % The number of collocation points
X=ME_points(N); % Collocation points as a vector with N *3 dimension
%% Constant parameters
E=1;       % gradient energy coefficient
dt=1e-8;  % time step
T=0.0001; % final time
NT=T/dt;  % number of time intervals
ep=10;     % RBF shape parameter
%% Normal vector at collocation points - not specific to the sphere
nr(:,1) = X(:,1)./sqrt(X(:,1).^2+X(:,2).^2+X(:,3).^2);
nr(:,2) = X(:,2)./sqrt(X(:,1).^2+X(:,2).^2+X(:,3).^2);
nr(:,3) = X(:,3)./sqrt(X(:,1).^2+X(:,2).^2+X(:,3).^2);
%% Compute the Surface Laplacian - not specific to the sphere
xij = repmat(X(:,1),[1 N]); xij=xij-xij.'; nxi=repmat(nr(:,1),[1 N]);
yij = repmat(X(:,2),[1 N]); yij=yij-yij.'; nyi=repmat(nr(:,2),[1 N]);
zij = repmat(X(:,3),[1 N]); zij=zij-zij.'; nzi=repmat(nr(:,3),[1 N]);
r = sqrt(xij.^2 + yij.^2 + zij.^2);
A = dphi(r,ep);
DPx = ((1-nxi.^2).*xij - nxi.*nyi.*yij - nxi.*nzi.*zij).*A;
DPy = (-nxi.*nyi.*xij + (1-nyi.^2).*yij - nyi.*nzi.*zij).*A;
DPz = (-nxi.*nzi.*xij - nyi.*nzi.*yij + (1-nzi.^2).*zij).*A;
A = chol(phi(r,ep)); Gx = (DPx/A)/A.'; Gy = (DPy/A)/A.'; Gz = (DPz/A)/A.';
LX = Gx*Gx+Gy*Gy+Gz*Gz;  % Surface Laplacian
%% Time integration - not specific to the sphere
U0 = Uexact(X(:,1),X(:,2),X(:,3),0);  % Initial condition
for n = 1:NT
    t = n*dt;
    Ustar = U0 + dt*LX*U0 + dt*f(X(:,1),X(:,2),X(:,3),t-dt,E);
    U0=Ustar./sqrt(exp(-2*dt/E^2)+(Ustar).^2.*(1-exp(-2*dt/E^2)));
end
%% Interpolate the solution to a grid on the sphere using RBFs
sph = @(la,th) [r*sin(la).*cos(th)  r*sin(la).*sin(th) r*cos(la)];
sz = [100 100]; M = prod(sz);  % surface grid parameters
[ll,tt] = meshgrid(linspace(0,pi,sz(2)),linspace(0,2*pi,sz(1)));
xx = sph(ll(:),tt(:));
re2 = (repmat(xx(:,1),[1 N])-repmat(X(:,1).',[M 1])).^2;
re2 = re2+(repmat(xx(:,2),[1 N])-repmat(X(:,2).',[M 1])).^2;
re2 = re2+(repmat(xx(:,3),[1 N])-repmat(X(:,3).',[M 1])).^2;
yy = reshape(xx(:,2),sz);
zz = reshape(xx(:,3),sz);
xx = reshape(xx(:,1),sz);
%% Figure of approximation solution on the sphere
uu = reshape(phi(sqrt(re2),ep)*(A\(A.'\U0)),sz);
figure, surf(xx,yy,zz,uu);
shading interp; daspect([1 1 1]);
```

References

1. Adalsteinsson, D., Sethian, J.A.: Transport and diffusion of material quantities on propagating interfaces via level set methods. J. Comput. Phys. **185**(1), 271–288 (2003)
2. Arcangli, R., Lpez de Silanes, M.C., Torrens, J.J.: An extension of a bound for functions in Sobolev spaces, with applications to (m, s)-spline interpolation and smoothing. Numer. Math. **107**(2), 181–211 (2007)

3. Arcangli, R., Lpez de Silanes, M.C., Torrens, J.J.: Extension of sampling inequalities to Sobolev seminorms of fractional order and derivative data. Numer. Math. **121**, 587–608 (2012)
4. Allen, S.M., Cahn, J.W.: A microscopic theory for antiphase boundary motion and its application to antiphase domain coarsening. Acta Metall. **27**, 1085–1095 (1979)
5. Beneš, M., Chalupecký, V., Mikula, K.: Geometrical image segmentation by the Allen-Cahn equation. Appl. Numer. Math. **51**, 187–205 (2004)
6. Besse, C., Bidégaray, B., Descombes, S.: Order estimates in time of splitting methods for the nonlinear Schrodinger equation. SIAM J. Numer. Anal. **40**, 26–40 (2002)
7. Bertalmo, M., Cheng, L., Osher, S., Sapiro, G.: Variational problems and partial differential equations on implicit surfaces. J. Comput. Phys. **174**, 759–780 (2001)
8. Calhoun, D.A., Helzel, C.: A finite volume method for solving parabolic equations on logically Cartesian curved surface meshes. SIAM J. Sci. Comput. **31**(6), 4066–4099 (2009)
9. Chen, L.Q.: Phase-field models for microstructure evolution. Annu. Rev. Mater. Res. **32**, 113–140 (2002)
10. Cheng, M., Warren, J.A.: An efficient algorithm for solving the phase field crystal model. J. Comput. Phys. **227**, 6241–6248 (2008)
11. Choi, Y., Jeong, D., Lee, S., Yoo, M., Kim, J.: Motion by mean curvature of curves on surfaces using the Allen-Cahn equation. Int. J. Eng. Sci. **97**, 126–132 (2015)
12. Csomós, P., Faragó, I.: Error analysis of the numerical solution of split differential equations. Math. Comput. Model. **48**, 1090–1106 (2008)
13. Dziuk, G.: Finite elements for the Beltrami operator on arbitrary surfaces. In: Hildebrandt, S., Leis, R. (eds.) Partial Differential Equations and Calculus of Variations. Lecture Notes in Mathematics, vol. 1357. Springer, Berlin (1988)
14. Dziuk, G., Elliot, C.: Finite elements on evolving surfaces. IMA J. Numer. Anal. **27**, 262–292 (2007)
15. Dziuk, G., Elliot, C.M.: Surface finite elements for parabolic equations. J. Comput. Math. **25**, 385–407 (2007)
16. Fasshauer, G.E.: Meshfree Approximation Methods with MATLAB. World Scientific, Hackensack (2007)
17. Feng, Z., Yin, J., Zhou, J.: Inpainting algorithm for jacquared image based on phase-field model. In: IEEE Intelligent System and Knowledge Engineering ISKE, pp. 1203–1207 (2008)
18. Flyer, N., Wright, G.B.: A radial basis function method for the shallow water equations on a sphere. Proc. R. Soc. A **465**, 1949–1976 (2009)
19. Flyer, N., Wright, G.B.: Transport schemes on a sphere using radial basis functions. J. Comput. Phys. **226**, 1059–1084 (2007)
20. Fuselier, E.J., Wright, G.B.: A high-order kernel method for diffusion and reaction-diffusion equations on surfaces. J. Sci. Comput. **56**(3), 535–565 (2013)
21. Fuselier, E.J., Wright, G.B.: Order-preserving derivative approximation with periodic radial basis functions. Adv. Comput. Math. **41**, 23–53 (2015)
22. Fuselier, E.J., Wright, G.B.: Scattered data interpolation on embedded submanifolds with retricted positive definite kernels: Sobolev error estimates. SIAM J. Numer. Anal. **50**(3), 1753–1776 (2012)
23. Kay, D.A., Tomasi, A.: Color image segmentation by the vector-valued Allen-Cahn phase-field model: a multigrid solution. IEEE Trans. Image Process. **18**, 2330–2339 (2009)
24. Kim, J., Lee, S., Choi, Y.: A conservative Allen-Cahn equation with a space-time dependent Lagrange multiplier. Int. J. Eng. Sci. **84**, 11–17 (2014)
25. Kim, J., Jeong, D., Yang, S.-D., Choi, Y.: A finite difference method for a conservative Allen-Cahn equation on non-flat surfaces. J. Comput. Phys. **334**, 170–181 (2017)
26. Kowalczyk, M.: On the existence and Morse index of solutions to the Allen-Cahn equation in two dimensions. Ann. Mat. Pura Appl. **184**, 17–52 (2005)
27. Le Gia, Q.T., Narcowich, F.J., Ward, J.D., Wendland, H.: Continuous and discrete least-squares approximation by radial basis functions on spheres. J. Approx. Theory **143**, 124–133 (2006)
28. Le Gia, Q.T.: Galerkin approximation for elliptic PDEs on spheres. J. Approx. Theory **130**, 123–147 (2004)
29. Le Gia, Q.T.: Multiscale RBF collocation for solving PDEs on spheres. Numer. Math. **121**, 99–125 (2012)
30. Lehto, E., Shankar, V., Wright, G.B.: A radial basis function (RBF) compact finite difference (FD) scheme for reaction-diffusion equations on surfaces SIAM. J. Sci. Comput **39**(5), 2129–2151 (2017)
31. Li, Y., Jeong, D., Choi, J., Lee, S., Kim, J.: Fast local image inpainting based on the Allen-Cahn model. Digit. Signal Process. **37**, 65–74 (2015)
32. Lee, H.G., Kim, J.: A simple and efficient finite difference method for the phase-field crystal equation on curved surfaces. Comput. Methods Appl. Mech. Eng. **307**, 32–43 (2016)
33. Macdonald, C.B., Ruuth, S.J.: Level set equations on surfaces via the closest point method. J. Sci. Comput. **35**, 219–240 (2008)

34. Mirzaei, D.: Direct approximation on spheres using generalized moving least squares. BIT Numer. Math. **57**, 1041–1063 (2017)
35. Mirzaei, D.: A Petrov-Galerkin kernel approximation on the sphere. SIAM J. Numer. Anal. **56**(1), 274–295 (2018)
36. Morton, T.M., Neamtu, M.: Error bonds for solving pseudodifferential equations on spheres. J. Approx. Theory **114**, 242–268 (2002)
37. Narcowich, F.J., Sun, X., Ward, J.D.: Approximation power of RBFs and their associated SBFs: a connection. Adv. Comput. Math. **27**, 107–124 (2007)
38. Narcowich, F.J., Ward, J.D., Wendland, H.: Sobolev bounds on functions with scattered zeros, with applications to radial basis function surface fitting. Math. Comput. **74**, 743–763 (2005)
39. Narcowich, F.J., Ward, J.D.: Scattered-data interpolation on spheres: error estimates and locally supported basis functions. SIAM J. Math. Anal. **33**, 1393–1410 (2002)
40. Narcowich, F.J., Rowe, S.T., Ward, J.D.: A novel Galerkin method for solving PDEs on the sphere using highly localized kernel bases. Math. Comput. **86**, 197–231 (2017)
41. Shankar, V., Wright, G.B., Fogelson, A.L., Kirby, R.M.: A radial basis function (RBF)-finite difference (FD) method for diffusion and reaction-diffusion equations on surfaces. J. Sci. Comput. **63**, 745–768 (2015)
42. Shen, J., Yang, X.: A phase-field model and its numerical approximation for two-phase incompressible flows with different densities and viscosities. SIAM J. Sci. Comput. **32**, 1159–1179 (2010)
43. Ward, M.J.: Metastable bubble solutions for the Allen-Cahn equation with mass conservation. SIAM J. Appl. Math. **56**, 1247–1279 (1996)
44. Wendland, H.: Scattered Data Approximation. Cambridge Mongraph on Applied and Computational Mathematics. Cambridge University Press, New York (2005)
45. Wendland, H.: Divergence-free kernel methods for approximating the Stokes problem. SIAM J. Numer. Anal. **47**(4), 3158–3179 (2009)
46. Wendland, H., Rieger, C.: Approximate interpolation with applications to selecting smoothing parameters. Numer. Math. **101**, 643–662 (2005)
47. Wu, X., Zwieten, G.J., Zee, K.G.: Stabilized second-order convex splitting schemes for Cahn-Hilliard models with application to diffuse-interface tumor-growth models. Int. J. Numer. Methods Biomed. Eng. **30**, 180–203 (2014)
48. Xiao, X., Feng, X., Yuan, J.: The stabilized semi-implicit finite element method for the surface Allen-Cahn equation. Discrete Contin. Dyn. Syst. Ser. B **22**, 2857–2877 (2017)